

Surgical Aggregation: Federated Class-Heterogeneous Learning

Pranav Kulkarni, Adway Kanhere, Paul H. Yi, and Vishwa S. Parekh

Abstract—The release of numerous chest x-ray datasets has spearheaded the development of deep learning models with expert-level performance. However, they have limited interoperability due to class-heterogeneity – a result of inconsistent labeling schemes and partial annotations. Therefore, it is challenging to leverage these datasets in aggregate to train models with a complete representation of abnormalities that may occur within the thorax. In this work, we propose surgical aggregation, a federated learning framework for aggregating knowledge from class-heterogeneous datasets and learn a model that can simultaneously predict the presence of all disease labels present across the datasets. We evaluate our method using simulated and real-world class-heterogeneous datasets across both independent and identically distributed (iid) and non-iid settings. Our results show that surgical aggregation outperforms current methods, has better generalizability, and is a crucial first step towards tackling class-heterogeneity in federated learning to facilitate the development of clinically-useful models using previously non-interoperable chest x-ray datasets.

Index Terms—Federated learning, class-heterogeneity, generalizability, client drift, chest x-ray

I. INTRODUCTION

Deep learning has revolutionized the field of radiology in recent years, especially for its utility in screening life-threatening conditions using chest x-rays (CXRs) [1]. As a result, numerous large-scale CXR datasets have been released for the purpose of training high-performing models with expert-level detection of diseases in the thorax [2]–[5]. Since each dataset is curated at different sites using different acquisition parameters and image processing techniques, large-scale CXR datasets are heterogeneous and not independently and identically distributed (iid). Moreover, these datasets are *class-heterogeneous* due to inconsistent labeling schemes and partial annotations. In other words, each dataset focuses only on detecting a subset of findings that could be present in a patient and annotations present in one dataset may not be present in another – limiting their interoperability. For example, the NIH Chest X-ray 14 and CheXpert datasets

This work was supported by the University of Maryland School of Medicine. (Corresponding Author: Vishwa S. Parekh.)

Pranav Kulkarni, Adway Kanhere, Paul H. Yi, and Vishwa S. Parekh are with the University of Maryland Medical Intelligent Imaging (UM2ii) Center, University of Maryland School of Medicine, Baltimore, MD 21201, USA (e-mail: pkulkarni@som.umaryland.edu; akanhere@som.umaryland.edu; pyi@som.umaryland.edu; vparekh@som.umaryland.edu).

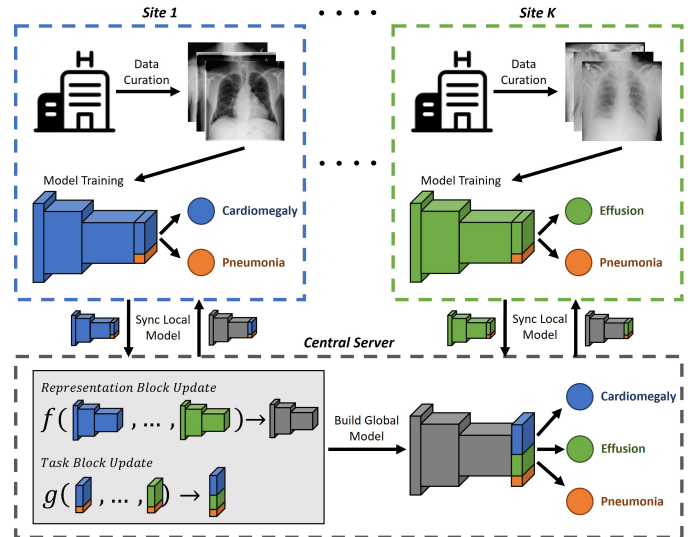


Fig. 1. An overview of surgical aggregation. Suppose two sites are curating CXR datasets to train models for their own niche applications; the first site works on cardiomegaly and pneumonia, while the second works on effusion and pneumonia. Using surgical aggregation, the central server aggregates “knowledge” from each site for their respective tasks to learn a global model that can detect all three tasks simultaneously.

contain 14 and 13 disease labels respectively, with only seven in common, making it challenging to leverage these datasets in aggregate to train large-scale models [2], [5].

Interoperability between these datasets is crucial as models trained on larger, diverse, multi-institutional datasets yield higher performance and better generalizability [6]–[8]. In the context of bias and fairness, models trained on multi-institutional datasets tend to the least biased towards underserved patient populations [9]. Therefore, there is a critically unmet need to address interoperability between large-scale CXR datasets, in order to train clinically-useful models with a complete representation of abnormalities that may occur in the thorax – even with the presence of class-heterogeneity.

In this work, we propose *surgical aggregation*, a semi-supervised federated learning framework for aggregating knowledge from class-heterogeneous datasets (Fig. 1). In the aforementioned example, surgical aggregation can leverage the NIH and CheXpert datasets in aggregate to train a large-scale model that can simultaneously predict the presence of all 20 unique disease labels across both datasets – while performing as well as models trained individually on both datasets. We validate our framework by conducting a series

of empirical experiments with varying levels of class- and data-heterogeneity to evaluate their stability using simulated iid datasets. Finally, we evaluate the efficacy of our framework in real-world settings using two large-scale non-iid datasets. Our main contributions are three-fold:

- 1) We propose a federated class-heterogeneous framework for training high-performing models that learn a complete representation of disease labels present across class-heterogeneous datasets.
- 2) Our extensive validation shows that surgical aggregation is stable to class- and data-heterogeneity and outperforms existing approaches.
- 3) We show that our framework has the potential to facilitate the development of large-scale models using previously non-interoperable datasets.

Our methods are detailed in Section III. Convergence analysis for surgical aggregation is in Section III-A.3. The experimental design is detailed in Section IV. Our results are detailed in Section V and discussed in Section VI. All our implementations are available on <https://github.com/UM2ii/SurgicalAggregation>.

II. RELATED WORK

The prevalent approach to leverage knowledge from the myriad of CXR datasets is training models individually on each dataset. While they yield high-performance in isolation, individually trained models often do not generalize well in the real-world due to domain shift [7], [8], [10]–[12]. Cohen *et al.* [6] demonstrated that the poor generalizability of individually trained models stemmed from not just shift in imaging data, but also from shift in labels due to factors like inconsistent labeling schemes and clinical biases. Furthermore, this siloed approach would result in an ever increasing number of models as more datasets get curated in the future for novel tasks (e.g., detection of COVID-19).

Various groups have explored the idea of leveraging multiple datasets in aggregate to yield high-performing and highly-generalizable models [6]–[9]. However, aggregating multi-site data in a centralized training setup is impractical due to patient data privacy. Federated learning (FL) was proposed as promising collaborative learning paradigm to mitigate this problem. Consisting of a central server with multiple clients, FL can train a global model on distributed datasets by aggregating "knowledge" (i.e., model weights) learned by local models at each client using a strategy like FedAvg [13], [14]. It has enabled training of large-scale models using medical imaging data distributed across multiple institutions without sharing sensitive patient data [14]–[16]. However, class- and data-heterogeneity pose a significant challenge to FL.

Due to data-heterogeneity, local models may learn features that differ significantly from each other (Fig. 2). Thus, different strategies have been proposed in literature for aggregating knowledge from non-iid datasets [17]–[21]. However, there is a significant gap in literature addressing class-heterogeneity. Most approaches focus on either detecting 1) the presence of an abnormality, or 2) the disease labels shared across all datasets [6]–[9]. Furthermore, most work by other groups in

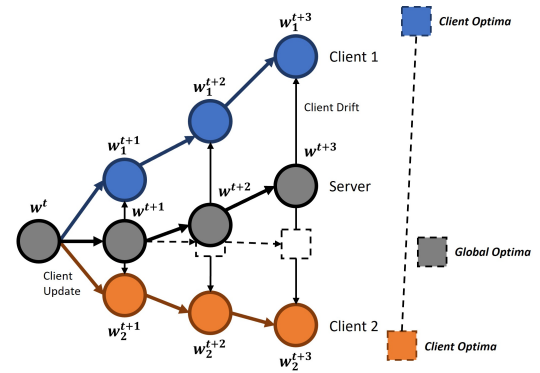


Fig. 2. Illustration of client drift in a FL setup in non-iid settings. As client model parameters move towards the client optima, the global model parameters drift away from the global optima for the network.

leveraging class-heterogeneous datasets to train models has been in a centralized setup [22]–[24].

Kulkarni *et al.* [25] explored a personalized FL (PFL) approach using two class-heterogeneous CXR datasets. However, PFL requires each client to learn a unique model and potentially results in ambiguous predictions from client-to-client and poor generalizability in the real-world [6], [26]. Gong *et al.* [27] proposed an ensemble attention distillation-based FL approach to train a global model using NIH and CheXpert datasets. However, this approach learns a multi-class classifier, i.e., the model can predict the presence of only one disease – even if other diseases may be present. Furthermore, an additional dataset is required for distillation at the central server. Dong *et al.* [28] developed a class-heterogeneous FL framework that used local consistency regularization to generate pseudo-labels for non-local classes at a client. However, this approach is dependent on the representation learned by the unsupervised pre-training step to generate low-uncertainty pseudo-labels – a crucial consideration for non-iid settings.

For segmentation, Miao *et al.* [29] proposed a class-heterogeneous FL framework that corrects local optimization by providing direction of gradient for non-local tasks using a modified cross-entropy loss. While segmentation is a fundamentally different problem than classification, the authors similarly noted a lack of prior literature for federated class-heterogeneous learning frameworks that leverage multiple datasets in aggregate to train a singular multi-task model.

Therefore, our proposed framework is different from prior work in three major aspects. First, our framework is capable of training a singular multi-label global model that can simultaneously predict the presence of more than one disease. Second, our framework is semi-supervised and does not require an additional dataset. Finally and most importantly, our framework does not require clients to know the tasks nor share the same tasks of other clients to participate in the network – a core assumption of most FL techniques [14]–[16].

III. METHODS

A. Surgical Aggregation

Surgical aggregation is a semi-supervised, model and task-agnostic FL framework for "stitching", i.e., selectively ag-

gregating, task-specific weights from all clients to construct a global task block for the global model – even with the presence of class-heterogeneity in the network. Our framework is built upon the premise that our method can leverage partially annotated class-heterogeneous datasets to learn a sufficiently good approximation of a model trained with a hypothetical fully annotated equivalent.

1) **Problem Setup:** Let us consider a FL setup comprising of $K \in \mathbb{N}$ clients (indexed by k) training for $T \in \mathbb{N}$ epochs with communication after every $E \in \mathbb{N}$ epochs, resulting in $\lfloor T/E \rfloor$ communication rounds. Furthermore, each client k has training data $\{\mathbf{x}_k, y_k\}$ with n_k samples.

Definition 1. We define a multi-label classifier as comprising of: 1) A representation block F consisting of feature extraction layers, and 2) a task block G consisting of fully-connected layers that interpret extracted features to predict classes, such that $\hat{y} = (G \circ F)(\mathbf{w}; \mathbf{x})$ for data $\{\mathbf{x}, y\}$.

Constraint 1. Let C denote the complete set of classes distributed across the network and C_k be the set of classes for client k , such that $C_k \subseteq C$ and $C = \bigcup_{k=1}^K C_k$.

Most FL approaches operate under the constraint that all classes are shared by all clients, i.e., $\forall c \in C_i, c \in C_j \forall i \neq j$. However, class-heterogeneity necessitates a broader definition:

Definition 2. We define class-heterogeneity as the case that covers: 1) Classes shared by all clients in the network, i.e., $\exists c \in C_i$ such that $c \in C_j \forall i \neq j$, 2) Classes partially shared by some clients in the network, i.e., $\exists c \in C_i$ such that $c \in C_j \exists i \neq j$, and 3) Classes unique to a client in the network, i.e., $\exists c \in C_i$ such that $c \notin C_j \forall i \neq j$.

2) **Algorithm Overview:** At the start of each communication round, clients train locally for E epochs before communicating the updated weights to the central server. The central server aggregates the weights of all layers in the representation block using strategy f (e.g., FedAvg). Our framework uses a modified aggregation strategy to construct a singular task block using task-specific weights from each client in the network.

As shown in Fig. 3, if a class is shared across one or more clients, the weights corresponding to the class in the task block are aggregated using strategy g . In our implementation, we

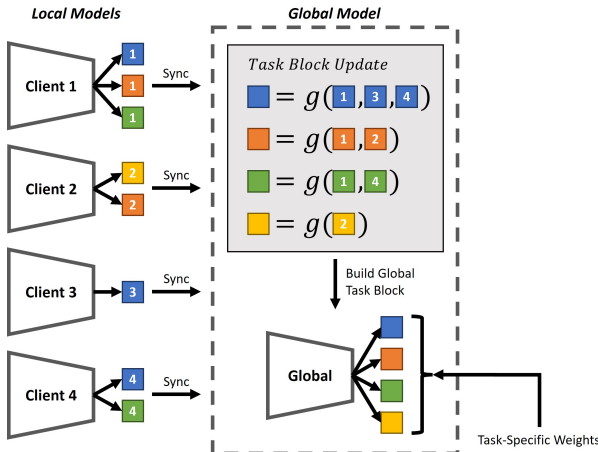


Fig. 3. Illustration of the surgical aggregation framework constructing a singular global task block using task-specific weights from each client in the network with task block aggregation strategy g (e.g., mean).

Algorithm 1: Surgical Aggregation

Input: K clients indexed by k with local tasks C_k , total epochs T , epochs before communication E , model layers indexed by l , initialized model parameters $\mathbf{w}_{0,k}^{(l)}$, representation block strategy f , task block strategy g ;

for each epoch $t \in \{1, 2, \dots, T\}$ **do**

for each client k and each layer l **do**

$\mathbf{w}_{t,k}^{(l)} \leftarrow \text{SGD}(\mathbf{w}_{t-1,k}^{(l)})$

end

if $\text{mod}(t, E) = 0$ **then**

for each client k and each layer l **do**

if layer l is not TaskBlock **then**

$\mathbf{w}_{t,k}^{(l)} \leftarrow f(\mathbf{w}_t^{(l)})$

else

for each class $c \in C_k$ **do**

$(\mathbf{w}_{t,k}^{(l)})_c \leftarrow g((\mathbf{w}_t^{(l)})_c)$

end

end

end

end

end

define g as the mean of task-specific weights. However, if a class is not shared with any other client, the weights remain unchanged. This strategy enables the selective aggregation of weights applied to the input of task block to construct a global task block to predict all C tasks in the network. The surgical aggregation framework is detailed in Algorithm 1.

3) **Convergence Analysis:** Let us consider a multi-label classifier with initialized parameters $\mathbf{w}_{0,k}$ updated using gradient descent. We primarily focus this convergence analysis on the modified strategy for task-specific weights in our method.

Definition 3. We define task-specific weights in the task block G as $(\mathbf{w}_{t,k}^{(G)})_c$, i.e., the weights corresponding to epoch $t \in [T]$ and client k for the class $c \in C_k$.

We analyze the convergence of surgical aggregation under scenarios of class-heterogeneity described in Definition 2.

Let $(G \circ F)(\mathbf{w})$ be the global model, while $(G \circ F)_k(\mathbf{w})$ be the local model for client k , such that our distributed optimization problem is defined as:

$$\min_{\mathbf{w}} \left\{ (G \circ F)^*(\mathbf{w}) \triangleq \frac{1}{K} \sum_{k=1}^K (G \circ F)_k^*(\mathbf{w}) \right\} \quad (1)$$

where the local objective $(G \circ F)_k^*$ is defined by:

$$(G \circ F)_k^* \triangleq \frac{1}{n_k} \sum_{i=1}^{n_k} L(\mathbf{w}, \mathbf{x}_{k,i}, y_{k,i}) \quad (2)$$

where L is the loss function (e.g., binary cross-entropy) [18].

Lemma 1. The optimization of the local objective $(G \circ F)_k^*$ for client k is controlled by the optimization of $(G \circ F)_k^*$ on each individual class $c \in C_k$.

Proof: For multi-label classifiers, the loss at client k is computed as the mean loss for each class $c \in C_k$ using loss

function L , such that:

$$L(\mathbf{w}, \mathbf{x}_{k,i}, y_{k,i}) = \frac{1}{|C_k|} \sum_{c \in C_k} \ell(\mathbf{w}, \mathbf{x}_{k,i}, (y_{k,i})_c) \quad (3)$$

where $(y_{k,i})_c$ is the ground truth for class c and sample $i \in [n_k]$ at client k . Therefore, to minimize $L(\mathbf{w}, \mathbf{x}_{k,i}, y_{k,i})$, $\ell(\mathbf{w}, \mathbf{x}_{k,i}, (y_{k,i})_c)$ must be minimized for all $c \in C_k$. In other words, optimizing $(G \circ F)_k^*$ on each individual class $c \in C_k$ ensures optimization of the local objective $(G \circ F)_k^*$.

Furthermore, the global objective $(G \circ F)^*$ can be interpreted as the optimization of two concurrent sub-objectives:

- 1) Optimizing the global representation block F by locally optimizing client representation blocks F_k , such that:

$$\min_{\mathbf{w}} \left\{ F^*(\mathbf{w}) \triangleq \frac{1}{K} \sum_{k=1}^K F_k^*(\mathbf{w}) \right\} \quad (4)$$

- 2) Optimizing the global task block G by locally optimizing client task blocks G_k , such that:

$$\min_{\mathbf{w}} \left\{ G^*(\mathbf{w}) \triangleq \frac{1}{K} \sum_{k=1}^K G_k^*(\mathbf{w}) \right\} \quad (5)$$

where the local sub-objectives $F_k^* = G_k^* \triangleq (G \circ F)_k^*$.

Lemma 2. *The optimization of the global sub-objective F^* is independent of class-heterogeneity present in the network.*

Proof: Like conventional FL approaches, in our approach the representation block weights $\mathbf{w}_{k,t}^{(F)}$ are always shared with all clients at the end of each communication round, such that:

$$\mathbf{w}_{t,k}^{(F)} = f(\mathbf{w}_t^{(F)}) \quad (6)$$

In this case, the convergence of $\mathbf{w}_{k,t}^{(F)}$ is well-established in prior literature [17], [18]. However, it is not clear whether class-heterogeneity affects the convergence of $\mathbf{w}_{k,t}^{(F)}$. The optimization of the global sub-objective F^* is controlled by the optimization of the local objective $(G \circ F)_k^*$. Therefore, the optimization of F^* is ensured if $F_k^* \triangleq (G \circ F)_k^*$ is optimized. While the optimization of $(G \circ F)_k^*$ is dependent on classes C_k , it is independent of the optimization of classes $c \in C \setminus C_k$ (Lemma 1). In other words, the optimization of F^* is driven by the optimization of F_k^* , regardless of any class-heterogeneity.

Since the task block weights are selectively aggregated, we analyze the convergence of the global task block (i.e., G^*) with respect to each individual class $c \in C$.

Lemma 3. *The optimization of the global objective $(G \circ F)^*$ with respect to a class $c \in C$, shared by a subset of clients K' , is controlled by the optimization of $(G \circ F)_k^*$ for all clients $k \in K'$ on the class c .*

Proof: Let K' be the subset of clients in the network sharing class $c \in C$. In our approach, the task-specific weights $(\mathbf{w}_{k,t}^{(G)})_c$ for clients $k \in K'$ are shared with the clients at the end of each communication round, such that:

$$(\mathbf{w}_{k,t}^{(G)})_c = g((\mathbf{w}_t^{(G)})_c) \quad (7)$$

The global sub-objective G^* with respect to the shared class c is controlled by the local optimization of G_k^* on class c for each clients $k \in K'$. Using Lemma 2, we conclude that with respect to shared class c , the optimization of global objective

$(G \circ F)^*$ is ensured. In other words, regardless of whether all or *some* clients share the class c , the $(G \circ F)^*$ is ensured to be optimized with respect to the class c .

We further analyze a special case for Lemma 3 where $|K'| = 1$, i.e., there is a class $c \in C$ unique to a client k .

Lemma 4. *The optimization of global objective $(G \circ F)^*$ with respect to a class $c \in C$, unique to client k , i.e., it is not shared by any other client in the network, is controlled by the optimization of $(G \circ F)_k^*$ on class c .*

Proof: The global sub-objective G^* with respect to the class c is by definition optimized by the local optimization of G_k^* on class c unique to client k . Using Lemma 2, we conclude that with respect to the class c , the optimization of the global objective $(G \circ F)^*$ is ensured.

Putting together Lemmas 3 and 4, we prove that the optimization of global objective $(G \circ F)^*$ with respect to class $c \in C$ is always ensured and is derived from previously established convergence analyses, regardless of class-heterogeneity in the network [17], [18]. Therefore, using Lemma 1, we can confer:

Theorem 1. *The optimization of global objective $(G \circ F)^*$ is ensured if local objective $(G \circ F)_k^*$ is optimized for all classes $c \in C_k$ using representation block strategy f and task block strategy g and optimization is independent of any class-heterogeneity present in the network.*

To conclude, Theorem 1 says that regardless of the class-heterogeneity present in the network, the convergence of surgical aggregation is guaranteed.

B. Comparison with Baselines

We compare our method to two baselines, i.e., models trained with well-established approaches in literature that represent an upper bound of the expected model performance, but do not yield a singular global model.

1) *Individually Trained Baseline:* The individually trained baseline refers to models trained individually on each dataset in a centralized setup using standard deep learning.

2) *PFL Baseline:* The PFL baseline encapsulates the growing popularity of personalized FL techniques in literature, where each client learns personalized local models in favor of generalized global models [17], [30], [31]. We implement the PFL baseline such that clients share a representation block, while learning a personalized task block for local classes.

C. Comparison with Existing Methods

We compare our method to three existing methods for training models by leveraging multiple datasets in aggregate. Unlike the baselines, these methods yield models with a singular task block.

1) *Centralized:* The centralized method refers to the well-established approach to achieve higher generalizability, where multiple datasets are concatenated locally to train a model in a centralized setup using standard deep learning [6]–[9]. All missing classes in the aggregated dataset are treated as negatives, i.e., $(y_i)_c = 0$ for all $c \in C \setminus C_k$.

2) *Vanilla FL:* The vanilla FL method is the conventional approach for FL where datasets are distributed across clients in the network [14]–[16]. Similar to the centralized method, missing classes in each dataset are treated as negatives.

3) *FL with Partial Loss*: The FL with partial loss method is a modification of the vanilla FL setup, inspired by methods for training multi-label classifiers with missing labels to tackle class-heterogeneity using a modified binary cross-entropy loss [22]–[24]. Jin *et al.* [22] defines the partial loss function for a client k with model parameters \mathbf{w} , local classes $C_k \subseteq C$, and local training data $\{\mathbf{x}_k, y_k\}$ containing n_k samples as follows:

$$L(\mathbf{w}, \mathbf{x}_{k,i}, y_{k,i}) = \frac{1}{|C_k|} \sum_{c \in C_k} \ell(\mathbf{w}, \mathbf{x}_{k,i}, (y_{k,i})_c) \quad (8)$$

D. Implementation

1) *Centralized Setup*: We use DenseNet121, pre-trained with ImageNet, to train multi-label classifiers using binary cross-entropy (BCE) loss with batch size of 64. Prior to training, task blocks are pre-trained using transfer learning for 15 epochs with learning rate of 5e-3, while keeping representation block weights frozen. Then, the model is fine-tuned for 150 epochs with learning rate of 5e-5.

2) *Federated Setup*: We simulate a FL setup using the above methods with $T = 150$ epochs and $E = 1$ epochs before communication, resulting in 150 communication rounds. Convergence of the global model is determined by the mean of local validation BCE loss for each client (Eq. 1). For each FL approach, we consider the three FL aggregation strategies:

- FedAvg, the de-facto FL strategy [13]
- FedBN, a variation of FedAvg with local batch normalization [17]. Since FedBN is designed primarily for PFL tasks, it is only included for the PFL baseline model.
- FedBN+, a modification of FedBN with pre-trained batch normalization statistics [32].

3) *Image Preprocessing*: All CXRs are downsampled to 224×224 , normalized between 0 and 1, and scaled to ImageNet statistics. Random augmentations (rotation, flip, zoom, and contrast) were applied to input images during training.

4) *Environment*: All models are trained and evaluated using TensorFlow (version 2.8.1) and CUDA (version 12.0) on four NVIDIA RTX A6000 GPUs.

IV. EXPERIMENTAL SETUP

A. Datasets

We use three large-scale CXR datasets that are class- and data-heterogeneous, as shown in Fig. 4.

1) *NIH Chest X-Ray 14*: The NIH Chest X-Ray 14 dataset consists of 14 disease labels with $n = 112,120$ frontal CXRs from 30,805 patients [5]. We randomly divide the dataset into training (70%, $n = 78,075$), validation (10%, $n = 11,079$), and testing (20%, $n = 22,966$) splits with no patient leakage.

2) *CheXpert*: The CheXpert dataset consists of 13 disease labels (seven shared with the NIH dataset) with $n = 224,316$ CXRs from 65,240 patients [2]. All lateral images are discarded to yield $n = 191,027$ frontal CXRs. Uncertain labels are treated as negatives. We randomly divide the dataset into training (70%, $n = 133,638$), validation (10%, $n = 18,855$), and testing (20%, $n = 38,534$) splits with no patient leakage.

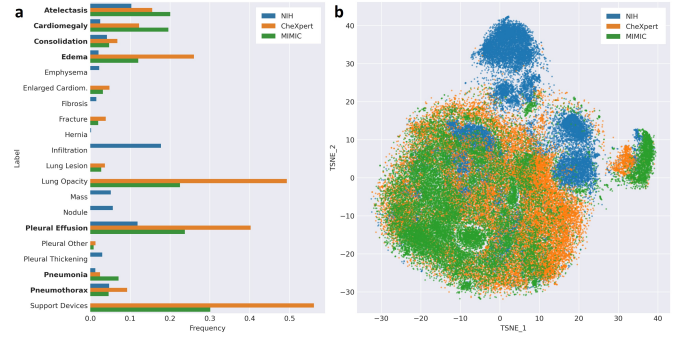


Fig. 4. Illustration of class- and data-heterogeneity between the NIH, CheXpert, and MIMIC-LT datasets. (a) Barplot showing class-heterogeneity between the three datasets as the frequency of occurrence of disease labels. The seven shared classes between the NIH and CheXpert datasets are highlighted in **bold**. The MIMIC-LT dataset contains all 20 classes. (b) Latent space representation showing data-heterogeneity between all three datasets using t-SNE [33].

3) *MIMIC-CXR-JPG*: The MIMIC-CXR-JPG dataset is used as our external test set to evaluate the generalizability to unseen data distributions [3], [34]. The MIMIC dataset consists of 13 disease labels (same as CheXpert) with $n = 377,110$ CXRs from 65,379 patients. All lateral images are discarded to yield $n = 243,324$ frontal CXRs. To thoroughly validate our method, we use the CXR-LT expanded set of 26 classes for the MIMIC dataset that provides ground truth for the 20 classes present across the NIH and CheXpert datasets as our fully annotated test set [34], [35].

B. Experiments

1) *Simulation Experiments*: We evaluate the effect of class- and data-heterogeneity using simulated datasets created by sampling iid subsets of the NIH dataset for each client, with varying levels of class- and data-heterogeneity, such that there is no patient leakage and all 14 classes from the NIH dataset appear at least once in each simulated dataset (Constraint 1).

Since each simulated dataset is an incomplete snapshot of the NIH dataset, we aim to empirically quantify how well our method approximates the performance of the NIH baseline, trained on fully annotated data (Section III). We evaluate our hypothesis across two sub-experiments:

First, we study the effect of data-heterogeneity across seven runs, each with an increasing number of clients $K \in \{2, 3, 4, 5, 6, 8, 10\}$ as a proxy for data-heterogeneity. As the number of clients increases, the sample size of the simulated dataset at each client decreases by factor of $1/K$, thus increasing statistical heterogeneity between clients. Second, we study the effect of class-heterogeneity across of seven runs, each with an increasing number of shared classes $\phi \in \{0, 2, 6, 10, 12, 13, 14\}$ as a proxy for class-heterogeneity. We keep the number of clients $K = 4$ and underlying imaging data at each client constant.

All models are evaluated on the held-out NIH test set and the external MIMIC-LT dataset. For all FL approaches, FedBN+ is used as the aggregation strategy. The PFL baseline is not included due to its inability to train singular multi-task models.

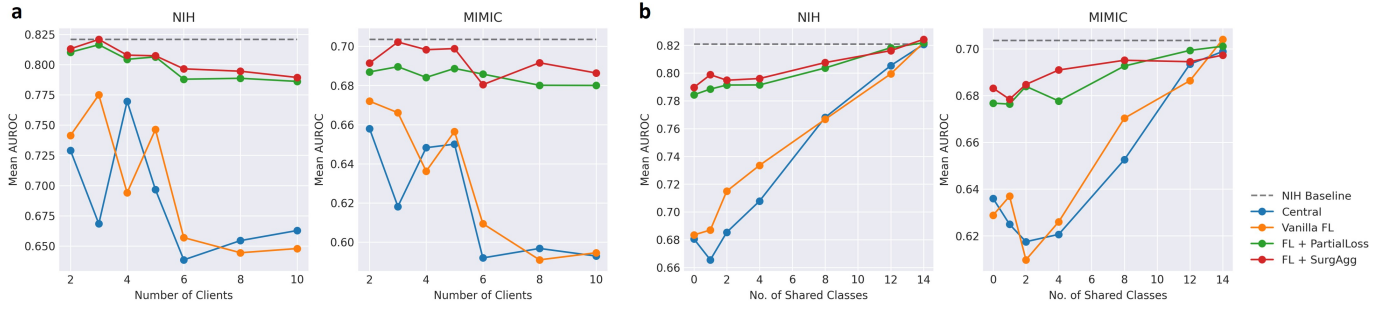


Fig. 5. Mean AUROC scores for iid simulation experiments across varying levels of class- and data-heterogeneity on the held-out NIH test set (left) and external MIMIC-LT dataset (right). (a) Effect of number of clients in the network as a proxy for data-heterogeneity. (b) Effect of number of shared classes across all clients in the network as a proxy for class-heterogeneity.

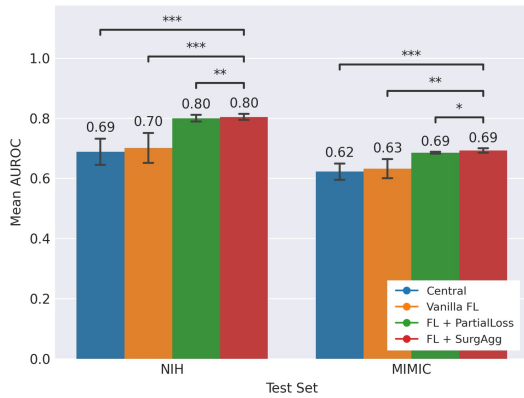


Fig. 6. Average mean AUROC scores for evaluating the effect of data-heterogeneity on the held-out NIH test set and external MIMIC-LT dataset using simulated iid datasets. Surgical aggregation is compared with existing methods for each test set using paired t-tests. ns: $p \geq 0.05$, *: $p < 0.05$, **: $p < 0.01$, ***: $p < 0.001$

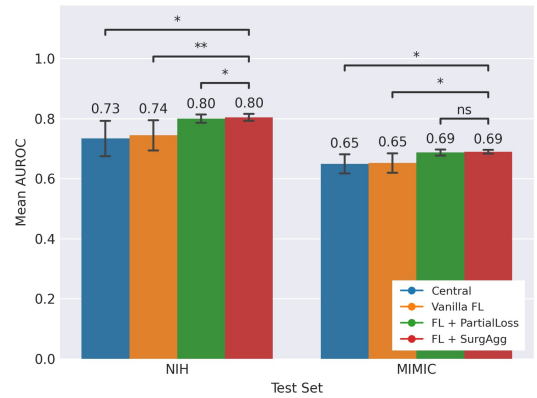


Fig. 7. Average mean AUROC scores for evaluating the effect of class-heterogeneity on the held-out NIH test set and external MIMIC-LT dataset using simulated iid datasets. Surgical aggregation is compared with existing methods for each test set using paired t-tests. ns: $p \geq 0.05$, *: $p < 0.05$, **: $p < 0.01$, ***: $p < 0.001$

2) *Real-World Experiments*: In addition to evaluating the stability of our framework across varying levels of class- and data-heterogeneity, we evaluate the efficacy of our framework in the real-world using two non-iid large-scale CXR datasets – NIH and CheXpert – to conduct two sub-experiments.

In the first sub-experiment, we consider the scenario without class-heterogeneity, an ideal scenario for existing FL setups, where only on the seven shared classes between both datasets are included as ground truth annotations (see Fig. 4). In the second experiment, we consider all classes to encapsulate a real-world class- and data-heterogeneous problem by training a model with a complete representation of all 20 classes across both datasets. All models are evaluated on the held-out NIH and CheXpert test sets and external MIMIC-LT dataset.

C. Metrics and Statistical Analyses

Model performance in a multi-label scenario is quantified by the mean of area under the receiver operating characteristic curve (AUROC) scores for each class in the test set. If a class in the test set is absent from the set of classes learned by a model, the mean AUROC score is not defined.

For the simulation experiments, performance between models is compared using paired t-tests between the mean AUROC scores to test for significance. For real-world experiments,

performance between models is compared using paired t-tests across the granular class-level AUROC scores to test for significance. In all cases, statistical significance was defined as $p < 0.05$ and the difference between paired samples is normal, indicated by $p \geq 0.05$ using the Shapiro-Wilk test.

V. RESULTS

A. Simulation Experiments

1) *Effect of Data-Heterogeneity*: Across varying levels of data-heterogeneity, we observe that surgical aggregation outperforms all existing methods with average mean AUROC 0.80 ± 0.01 on the held-out NIH test set (all $p < 0.005$). While FL with partial loss performs comparably to our method, the difference in average mean AUROCs (margin 0.004) is statistically significant ($p = 0.004$). On the external MIMIC-LT dataset, our method generalizes better with average mean AUROC 0.69 ± 0.01 , compared to all existing methods (all $p < 0.03$). Results are detailed in Figs. 5(a) and 6.

2) *Effect of Class-Heterogeneity*: Across varying levels of class-heterogeneity, with constant data-heterogeneity, we observe that surgical aggregation outperforms all existing methods with average mean AUROC 0.80 ± 0.01 on the held-out NIH test set (all $p < 0.03$). Similarly, the minor differences in average mean AUROCs between FL with partial loss and

TABLE I

MEAN AUROC SCORES ON THE HELD-OUT NIH AND CHEXPert TEST SETS AND EXTERNAL MIMIC-LT DATASET FOR REAL-WORLD EXPERIMENT WITHOUT CLASS-HETEROGENEITY. ALL VALUES REPORTED AS MEAN \pm SD. BEST PERFORMING METHOD IS HIGHLIGHTED IN **BOLD**. SURGICAL AGGREGATION IS COMPARED WITH EXISTING METHODS FOR EACH TEST SET USING PAIRED T-TESTS.

	NIH	CheXpert	MIMIC-LT
NIH Baseline	0.84 \pm 0.05 ^{ns}	0.70 \pm 0.07 ^{**}	0.73 \pm 0.10 ^{**}
CheXpert Baseline	0.81 \pm 0.06 [*]	0.76 \pm 0.07 ^{ns}	0.75 \pm 0.09 ^{ns}
PFL Baseline			
FedAvg	0.83 \pm 0.06 [*]	0.76 \pm 0.07 ^{ns}	0.76 \pm 0.09 ^{ns}
FedBN	0.83 \pm 0.05 [*]	0.77 \pm 0.07 ^{ns}	0.75 \pm 0.08 ^{ns}
FedBN+	0.83 \pm 0.06 ^{**}	0.76 \pm 0.07 ^{ns}	0.75 \pm 0.08 ^{ns}
Central	0.82 \pm 0.06 ^{**}	0.77 \pm 0.07 ^{ns}	0.76 \pm 0.10 ^{ns}
Vanilla FL			
FedAvg	0.81 \pm 0.05 ^{***}	0.74 \pm 0.08 [*]	0.74 \pm 0.10 [*]
FedBN+	0.84 \pm 0.05 [*]	0.75 \pm 0.08 [*]	0.75 \pm 0.09 ^{ns}
FL + PartialLoss			
FedAvg	0.82 \pm 0.05 ^{***}	0.75 \pm 0.08 [*]	0.74 \pm 0.10 [*]
FedBN+	0.83 \pm 0.06 [*]	0.75 \pm 0.07 ^{ns}	0.76 \pm 0.09 ^{ns}
FL + SurgAgg			
FedAvg	0.84 \pm 0.05 [*]	0.75 \pm 0.07 ^{ns}	0.75 \pm 0.09 ^{ns}
FedBN+	0.84 \pm 0.06	0.77 \pm 0.08	0.76 \pm 0.10

ns: $p \geq 0.05$, *: $p < 0.05$, **: $p < 0.01$, ***: $p < 0.001$

surgical aggregation are statistically significant (margin 0.004, $p = 0.03$). On the external MIMIC-LT dataset, our method generalizes better than all existing methods with average mean AUROC 0.69 ± 0.01 . Results are detailed in Figs. 5(b) and 7.

Finally, across both sub-experiments, our results indicate that even with varying levels of class- and data-heterogeneity in the network, surgical aggregation provides the closest approximation to the performance of the NIH baseline model (mean AUROC 0.82, mean margin 0.017), followed by FL with partial loss as a close second (mean margin 0.021).

B. Real-World Experiments

1) *Data-Heterogeneous Scenario*: We observe that the purely data-heterogeneous scenario results in similar mean AUROCs across the held-out NIH and CheXpert test sets and the external MIMIC-LT dataset. This implies that surgical aggregation is comparable to current FL approaches in the absence of class-heterogeneity (Table I).

Specifically, on the NIH test set, surgical aggregation performs comparably to the NIH baseline with mean AUROC 0.84 ± 0.06 ($p = 0.22$), while outperforming other baselines (all $p < 0.03$) and existing methods (all $p < 0.02$).

On the CheXpert test set, surgical aggregation performs comparably to the CheXpert baseline model with mean AUROC 0.77 ± 0.08 ($p = 0.51$). Our method performs on par with the PFL baselines (all $p > 0.05$) and existing methods, while outperforming the NIH baseline ($p = 0.002$).

Finally, on the external MIMIC-LT dataset, we observe that surgical aggregation’s generalizability to unseen data is on par with baselines with mean AUROC 0.76 ± 0.10 (all $p > 0.05$), with the exception of the NIH baseline ($p = 0.009$). Similarly, our method performs comparably to the existing methods.

2) *Class- and Data-Heterogeneous Scenario*: We observe that the introduction of class-heterogeneity results in a severe degradation of model performance for the existing methods,

TABLE II

MEAN AUROC SCORES ON THE HELD-OUT NIH AND CHEXPert TEST SETS AND EXTERNAL MIMIC-LT DATASET FOR REAL-WORLD EXPERIMENT WITH CLASS-HETEROGENEITY. ALL VALUES REPORTED AS MEAN \pm SD. BEST PERFORMING METHOD IS HIGHLIGHTED IN **BOLD**. SURGICAL AGGREGATION IS COMPARED WITH EXISTING METHODS FOR EACH TEST SET USING PAIRED T-TESTS.

	NIH	CheXpert	MIMIC-LT
NIH Baseline	0.82 \pm 0.06 ^{ns}	-	-
CheXpert Baseline	-	0.74 \pm 0.07 [*]	-
PFL Baseline			
FedAvg	0.79 \pm 0.07 ^{***}	0.73 \pm 0.07 ^{***}	-
FedBN	0.81 \pm 0.06 ^{ns}	0.74 \pm 0.06 [*]	-
FedBN+	0.81 \pm 0.06 ^{ns}	0.73 \pm 0.07 [*]	-
Central	0.71 \pm 0.13 ^{**}	0.72 \pm 0.07 ^{***}	0.65 \pm 0.10 ^{***}
Vanilla FL			
FedAvg	0.70 \pm 0.10 ^{***}	0.68 \pm 0.08 ^{***}	0.64 \pm 0.09 ^{***}
FedBN+	0.71 \pm 0.12 ^{***}	0.68 \pm 0.09 ^{***}	0.66 \pm 0.10 ^{***}
FL + PartialLoss			
FedAvg	0.77 \pm 0.09 ^{***}	0.68 \pm 0.07 ^{***}	0.68 \pm 0.09 ^{***}
FedBN+	0.78 \pm 0.07 ^{***}	0.71 \pm 0.07 ^{***}	0.68 \pm 0.09 ^{***}
FL + SurgAgg			
FedAvg	0.80 \pm 0.06 [*]	0.73 \pm 0.07 ^{**}	0.70 \pm 0.09 ^{ns}
FedBN+	0.81 \pm 0.07	0.76 \pm 0.08	0.71 \pm 0.10

ns: $p \geq 0.05$, *: $p < 0.05$, **: $p < 0.01$, ***: $p < 0.001$

while the baseline methods demonstrate high-performance. Our results show that surgical aggregation continues to yield high-performance (Table II).

Specifically, on the NIH test set, surgical aggregation performs comparably to the baseline models with mean AUROC 0.81 ± 0.07 (all $p > 0.05$), apart from the FedAvg PFL baseline ($p < 0.001$). Furthermore, our method outperforms the existing methods (all $p < 0.002$). On the CheXpert test set, surgical aggregation outperforms all baselines (all $p < 0.03$) and existing methods (all $p < 0.004$) with mean AUROC 0.76 ± 0.08 . Finally, on the external MIMIC-LT dataset, surgical aggregation outperforms all existing methods with mean AUROC 0.71 ± 0.10 (all $p < 0.001$).

We further explore the performance on a granular level by measuring the mean AUROC scores of the shared and the unique classes for the held-out NIH and CheXpert test sets (Table III). We observe that the existing methods perform poorly on the unique classes when compared to the baselines. In stark contrast, surgical aggregation demonstrates high-performance on the unique classes. On the NIH test set, our method performs on par with the baselines ($p > 0.05$), but on the CheXpert test set, surgical aggregation performs comparably to the baselines on the shared classes (both $p > 0.05$), while outperforming them on the unique classes (both $p < 0.008$).

Since the mean AUROC scores for baselines are not defined on the expanded MIMIC-LT classes, we explore generalizability by measuring mean AUROC scores of the NIH and CheXpert classes separately on the external MIMIC-LT dataset (Table IV). We observe that surgical aggregation generalizes better than the baselines and existing methods on NIH classes with mean AUROC 0.76 ± 0.10 (all $p < 0.006$). Similarly, on CheXpert classes, our method yields mean AUROC 0.70 ± 0.12 and outperforms the existing methods (all $p < 0.02$), while performing comparably to the baselines (all $p > 0.05$), except the CheXpert baseline ($p = 0.04$).

TABLE III

SUB-ANALYSIS OF MEAN AUROC SCORES FOR SHARED AND UNIQUE CLASSES (FIG. 4) ON THE HELD-OUT NIH AND CHEXPART TEST SETS FOR REAL-WORLD EXPERIMENT WITH CLASS-HETEROGENEITY. ALL VALUES REPORTED AS MEAN \pm SD. BEST PERFORMING METHOD IS HIGHLIGHTED IN **BOLD**. SURGICAL AGGREGATION IS COMPARED WITH EXISTING METHODS FOR EACH TEST SET AND SUB-GROUP USING PAIRED T-TESTS.

	NIH		CheXpert	
	Shared Classes	Unique Classes	Shared Classes	Unique Classes
NIH Baseline	0.84 \pm 0.06 ^{ns}	0.80 \pm 0.07 ^{ns}	0.70 \pm 0.08 ^{**}	-
CheXpert Baseline	0.81 \pm 0.07 [*]	-	0.76 \pm 0.07 ^{ns}	0.71 \pm 0.05 ^{**}
PFL Baseline	0.83 \pm 0.06 ^{**}	0.80 \pm 0.07 ^{ns}	0.76 \pm 0.07 ^{ns}	0.70 \pm 0.05 ^{**}
Central	0.82 \pm 0.05 [*]	0.60 \pm 0.07 ^{***}	0.74 \pm 0.07 ^{ns}	0.69 \pm 0.06 ^{**}
Vanilla FL	0.82 \pm 0.06 ^{**}	0.60 \pm 0.06 ^{***}	0.73 \pm 0.09 ^{**}	0.62 \pm 0.05 ^{**}
FL + PartialLoss	0.82 \pm 0.05 [*]	0.73 \pm 0.06 ^{***}	0.74 \pm 0.07 [*]	0.67 \pm 0.04 ^{**}
FL + SurgAgg	0.84 \pm 0.06	0.78 \pm 0.07	0.77 \pm 0.09	0.75 \pm 0.07

ns: $p \geq 0.05$, *: $p < 0.05$, **: $p < 0.01$, ***: $p < 0.001$

TABLE IV

SUB-ANALYSIS OF MEAN AUROC SCORES FOR NIH AND CHEXPART CLASSES ON THE EXTERNAL MIMIC-LT DATASET FOR REAL-WORLD EXPERIMENT WITH CLASS-HETEROGENEITY. ALL VALUES REPORTED AS MEAN \pm SD. BEST PERFORMING METHOD IS HIGHLIGHTED IN **BOLD**. SURGICAL AGGREGATION IS COMPARED WITH EXISTING METHODS FOR EACH TEST SET USING PAIRED T-TESTS.

	MIMIC-LT	
	NIH Classes	CheXpert Classes
NIH Baseline	0.73 \pm 0.10 ^{**}	-
CheXpert Baseline	-	0.67 \pm 0.11 [*]
PFL Baseline		
FedAvg	0.74 \pm 0.11 ^{***}	0.69 \pm 0.10 ^{ns}
FedBN	0.70 \pm 0.09 ^{***}	0.67 \pm 0.10 ^{ns}
FedBN+	0.74 \pm 0.10 ^{**}	0.68 \pm 0.11 ^{ns}
Central	0.74 \pm 0.09 ^{**}	0.66 \pm 0.11 ^{**}
Vanilla FL		
FedAvg	0.72 \pm 0.10 ^{***}	0.62 \pm 0.06 ^{**}
FedBN+	0.75 \pm 0.10 ^{**}	0.63 \pm 0.08 [*]
FL + PartialLoss		
FedAvg	0.74 \pm 0.09 ^{**}	0.66 \pm 0.09 [*]
FedBN+	0.74 \pm 0.10 ^{**}	0.64 \pm 0.10 [*]
FL + SurgAgg		
FedAvg	0.75 \pm 0.09 ^{ns}	0.68 \pm 0.10 ^{ns}
FedBN+	0.76 \pm 0.10	0.70 \pm 0.12

ns: $p \geq 0.05$, *: $p < 0.05$, **: $p < 0.01$, ***: $p < 0.001$

VI. DISCUSSION

Although the release of countless CXR datasets has spearheaded the utility of deep learning for expert-level detection of diseases in the thorax, the lack of interoperability due to class-heterogeneity has limited their utility beyond training "narrowly" focused models. Therefore, there is a significant gap in literature for methods that address class-heterogeneity and enable training of large-scale models by leveraging non-interoperable datasets in aggregate.

Our results demonstrate that surgical aggregation enables interoperability between distributed class-heterogeneous datasets to collaboratively develop a global multi-task model. In the absence of class-heterogeneity, surgical aggregation performs on par with well-established approaches in literature. However, in the presence of class-heterogeneity, our method continues to maintain high-performance and performs on par with, or in some cases outperforms, the baselines. More importantly, in the presence of class-heterogeneity, surgical aggregation scales well across both iid and non-iid settings. On the other

hand, existing methods fall short and scale poorly in non-iid settings. For example, while FL with partial loss is a close second in terms of performance with iid data, its performance significantly degrades with non-iid data. This is primarily due to feature shift between task-specific weights at each client as local updates from a client for non-local classes leads to client drift and degradation of performance on non-shared classes [6], [17]. Therefore, the selective aggregation of task-specific weights is critical to tackle class-heterogeneity in non-iid settings and is the crux of our method.

Another advantage of surgical aggregation is its ability to learn a singular multi-task global model that can predict the complete set of classes observed in the network. In stark contrast, the PFL paradigm entails K clients learning K personalized models. While it is popular approach to tackle non-iid data, PFL has interesting implications in the clinical environment. First, each personalized model will yield different predictions for the same CXR, thus, raising the question of which model's prediction should be trusted. Second, PFL emphasizes local optimization over generalization, thus making personalized models susceptible to poor generalizability on unseen data and shift in labeling schemes [6], [26].

These advantages enable surgical aggregation to not just facilitate greater collaboration between institutes focusing on different tasks in the same domain, but also enable the countless "narrowly" focused datasets (e.g., those curated for competitions) to be leveraged to collectively train clinically-useful models with a complete representation of abnormalities.

Despite our results demonstrating the advantages of surgical aggregation, our work has certain limitations. First, surgical aggregation is designed primarily for multi-label classifiers and may not scale for medical image segmentation – a fundamentally different and more difficult problem to solve. Second, due to limited literature for class-heterogeneous settings in FL, there are no established benchmarks to compare our method against beyond external validation. Third, our method requires all clients to share the same architecture for the representation block, an important consideration for clients with different computational resources. Finally, the empirical experiments are conducted on a simulated FL setup – lacking validation in real-world FL networks. For future work, we intend to explore solutions for these limitations and further validate our framework for real-world applications.

VII. CONCLUSION

Surgical aggregation is a crucial first step towards tackling class-heterogeneity in FL, especially between large-scale CXR datasets. Our results show that surgical aggregation can train high-performing models that simultaneously predict the presence of all disease labels present across the datasets and facilitate the development of highly-generalizable models using previously non-interoperable CXR datasets.

REFERENCES

- [1] M. P. McBee, O. A. Awan, A. T. Colucci, C. W. Ghobadi, N. Kadom, A. P. Kansagra, S. Tridandapani, and W. F. Auffermann, "Deep learning in radiology," *Academic radiology*, vol. 25, no. 11, pp. 1472–1480, 2018.
- [2] J. Irvin, P. Rajpurkar, M. Ko, Y. Yu, S. Ciurea-Ilcus, C. Chute, H. Marklund, B. Haghgoo, R. Ball, K. Shpanskaya, *et al.*, "Chexpert: A large chest radiograph dataset with uncertainty labels and expert comparison," in *Proceedings of the AAAI conference on artificial intelligence*, vol. 33, pp. 590–597, 2019.
- [3] A. E. Johnson, T. J. Pollard, N. R. Greenbaum, M. P. Lungren, C.-y. Deng, Y. Peng, Z. Lu, R. G. Mark, S. J. Berkowitz, and S. Horng, "Mimic-cxr-jpg, a large publicly available database of labeled chest radiographs," *arXiv preprint arXiv:1901.07042*, 2019.
- [4] H. Q. Nguyen, K. Lam, L. T. Le, H. H. Pham, D. Q. Tran, D. B. Nguyen, D. D. Le, C. M. Pham, H. T. Tong, D. H. Dinh, *et al.*, "Vindr-cxr: An open dataset of chest x-rays with radiologist's annotations," *Scientific Data*, vol. 9, no. 1, pp. 1–7, 2022.
- [5] X. Wang, Y. Peng, L. Lu, Z. Lu, M. Bagheri, and R. M. Summers, "Chestx-ray8: Hospital-scale chest x-ray database and benchmarks on weakly-supervised classification and localization of common thorax diseases," in *Proceedings of the IEEE conference on computer vision and pattern recognition*, pp. 2097–2106, 2017.
- [6] J. P. Cohen, M. Hashir, R. Brooks, and H. Bertrand, "On the limits of cross-domain generalization in automated x-ray prediction," in *Medical Imaging with Deep Learning*, pp. 136–155, PMLR, 2020.
- [7] E. H. Pooch, P. Ballester, and R. C. Barros, "Can we trust deep learning based diagnosis? the impact of domain shift in chest radiograph classification," in *Thoracic Image Analysis: Second International Workshop, TIA 2020, Held in Conjunction with MICCAI 2020, Lima, Peru, October 8, 2020, Proceedings 2*, pp. 74–83, Springer, 2020.
- [8] L. Yao, J. Prosky, B. Covington, and K. Lyman, "A strong baseline for domain adaptation and generalization in medical imaging," *arXiv preprint arXiv:1904.01638*, 2019.
- [9] L. Seyyed-Kalantari, H. Zhang, M. B. McDermott, I. Y. Chen, and M. Ghassemi, "Underdiagnosis bias of artificial intelligence algorithms applied to chest radiographs in under-served patient populations," *Nature medicine*, vol. 27, no. 12, pp. 2176–2182, 2021.
- [10] H. Guan and M. Liu, "Domain adaptation for medical image analysis: a survey," *IEEE Transactions on Biomedical Engineering*, vol. 69, no. 3, pp. 1173–1185, 2021.
- [11] D. C. Castro, I. Walker, and B. Glocker, "Causality matters in medical imaging," *Nature Communications*, vol. 11, no. 1, p. 3673, 2020.
- [12] O. Kilim, A. Olar, T. Joó, T. Palicz, P. Pollner, and I. Csabai, "Physical imaging parameter variation drives domain shift," *Scientific Reports*, vol. 12, no. 1, p. 21302, 2022.
- [13] B. McMahan, E. Moore, D. Ramage, S. Hampson, and B. A. y Arcas, "Communication-efficient learning of deep networks from decentralized data," in *Artificial intelligence and statistics*, pp. 1273–1282, PMLR, 2017.
- [14] A. Chowdhury, H. Kassem, N. Padoy, R. Umeton, and A. Karargyris, "A review of medical federated learning: Applications in oncology and cancer research," in *International MICCAI Brainlesion Workshop*, pp. 3–24, Springer, 2022.
- [15] N. Rieke, J. Hancox, W. Li, F. Milletari, H. R. Roth, S. Albarqouni, S. Bakas, M. N. Galtier, B. A. Landman, K. Maier-Hein, *et al.*, "The future of digital health with federated learning," *NPJ digital medicine*, vol. 3, no. 1, pp. 1–7, 2020.
- [16] M. J. Sheller, B. Edwards, G. A. Reina, J. Martin, S. Pati, A. Kotrotsou, M. Milchenko, W. Xu, D. Marcus, R. R. Colen, *et al.*, "Federated learning in medicine: facilitating multi-institutional collaborations without sharing patient data," *Scientific reports*, vol. 10, no. 1, p. 12598, 2020.
- [17] X. Li, M. Jiang, X. Zhang, M. Kamp, and Q. Dou, "Fedbn: Federated learning on non-iid features via local batch normalization," *arXiv preprint arXiv:2102.07623*, 2021.
- [18] X. Li, K. Huang, W. Yang, S. Wang, and Z. Zhang, "On the convergence of fedavg on non-iid data," *arXiv preprint arXiv:1907.02189*, 2019.
- [19] D. Li and J. Wang, "Fedmd: Heterogenous federated learning via model distillation," *arXiv preprint arXiv:1910.03581*, 2019.
- [20] Q. Li, B. He, and D. Song, "Model-contrastive federated learning," in *Proceedings of the IEEE/CVF conference on computer vision and pattern recognition*, pp. 10713–10722, 2021.
- [21] S. P. Karimireddy, S. Kale, M. Mohri, S. Reddi, S. Stich, and A. T. Suresh, "Scaffold: Stochastic controlled averaging for federated learning," in *International conference on machine learning*, pp. 5132–5143, PMLR, 2020.
- [22] R. Jin and Z. Ghahramani, "Learning with multiple labels," *Advances in neural information processing systems*, vol. 15, 2002.
- [23] S. S. Bucak, R. Jin, and A. K. Jain, "Multi-label learning with incomplete class assignments," in *CVPR 2011*, pp. 2801–2808, IEEE, 2011.
- [24] H. Wen, J. Cui, H. Hang, J. Liu, Y. Wang, and Z. Lin, "Leveraged weighted loss for partial label learning," in *International Conference on Machine Learning*, pp. 11091–11100, PMLR, 2021.
- [25] P. Kulkarni, A. Kanhere, P. H. Yi, and V. S. Parekh, "From competition to collaboration: Making toy datasets on kaggle clinically useful for chest x-ray diagnosis using federated learning," *arXiv preprint arXiv:2211.06212*, 2022.
- [26] R. Zhang, Z. Fan, Q. Xu, J. Yao, Y. Zhang, and Y. Wang, "Grace: A generalized and personalized federated learning method for medical imaging," in *International Conference on Medical Image Computing and Computer-Assisted Intervention*, pp. 14–24, Springer, 2023.
- [27] X. Gong, A. Sharma, S. Karanam, Z. Wu, T. Chen, D. Doermann, and A. Innanje, "Ensemble attention distillation for privacy-preserving federated learning," in *Proceedings of the IEEE/CVF International Conference on Computer Vision*, pp. 15076–15086, 2021.
- [28] N. Dong, M. Kampffmeyer, I. Voiculescu, and E. Xing, "Federated partially supervised learning with limited decentralized medical images," *IEEE Transactions on Medical Imaging*, 2022.
- [29] J. Miao, Z. Yang, L. Fan, and Y. Yang, "Fedseg: Class-heterogeneous federated learning for semantic segmentation," in *Proceedings of the IEEE/CVF Conference on Computer Vision and Pattern Recognition*, pp. 8042–8052, 2023.
- [30] P. P. Liang, T. Liu, L. Ziyin, N. B. Allen, R. P. Auerbach, D. Brent, R. Salakhutdinov, and L.-P. Morency, "Think locally, act globally: Federated learning with local and global representations," *arXiv preprint arXiv:2001.01523*, 2020.
- [31] A. Z. Tan, H. Yu, L. Cui, and Q. Yang, "Towards personalized federated learning," *IEEE Transactions on Neural Networks and Learning Systems*, 2022.
- [32] P. Kulkarni, A. Kanhere, P. H. Yi, and V. S. Parekh, "Fedbn+: Federated learning on heterogeneous datasets with pre-trained batch normalization," *arXiv preprint arXiv:2303.06180*, 2023.
- [33] L. Van der Maaten and G. Hinton, "Visualizing data using t-sne," *Journal of machine learning research*, vol. 9, no. 11, 2008.
- [34] A. L. Goldberger, L. A. Amaral, L. Glass, J. M. Hausdorff, P. C. Ivanov, R. G. Mark, J. E. Mietus, G. B. Moody, C.-K. Peng, and H. E. Stanley, "Physiobank, physiotoolkit, and physionet: components of a new research resource for complex physiologic signals," *circulation*, vol. 101, no. 23, pp. e215–e220, 2000.
- [35] G. Holste, Z. Jiang, A. Jaiswal, M. Hanna, S. Minkowitz, A. C. Legasto, J. G. Escalon, S. Steinberger, M. Bittman, T. C. Shen, *et al.*, "How does pruning impact long-tailed multi-label medical image classifiers?," in *International Conference on Medical Image Computing and Computer-Assisted Intervention*, pp. 663–673, Springer, 2023.